THE EUROPEAN
PHYSICAL JOURNAL PLUS

COVID-19 multiwaves as multiphase percolation: a general N-sigmoidal equation to model the spread

Ahmed El Aferni[1]**, Moez Guettari**[1,a] **, Abdelkader Hamdouni**[2]

[1] Preparatory Institute of Engineering of Tunis. Materials and Fluids Laboratory, University of Tunis, Tunis, Tunisia
[2] The Higher Institute of Sciences and Technologies of the Environnent Borj Cedria, University of Carthage, Carthage, Tunisia

Abstract The aim of the current study is to investigate the spread of the COVID-19 pandemic as a multiphase percolation process. Mathematical equations have been developed to describe the time dependence of the number of cumulative infected individuals, $I(t)$, and the velocity of the pandemic, $V_p(t)$, as well as to calculate epidemiological characteristics. The study focuses on the use of sigmoidal growth models to investigate multiwave COVID-19. Hill, logistic dose response and sigmoid Boltzmann models fitted successfully a pandemic wave. The sigmoid Boltzmann model and the dose response model were found to be effective in fitting the cumulative number of COVID-19 cases over time 2 waves spread ($N = 2$). However, for multiwave spread ($N > 2$), the dose response model was found to be more suitable due to its ability to overcome convergence issues. The spread of N successive waves has also been described as multiphase percolation with a period of pandemic relaxation between two successive waves.

1 Introduction

Modeling the spread of a pandemic allows us to analyze and predict its temporary evolution and examine the effect of different parameters such as the climate effect [1], environmental factors [2], epidemiological factors [3], and population density [4]. Since 2019, the World Health Organization (WHO) has declared the epidemic of coronavirus, SARS-CoV-2, as a global pandemic. As of September 20, 2022, the number of infected persons and deaths caused by SARS-CoV-2 has reached 617.749.410 and 6.532.317, respectively, worldwide [5]. Despite efforts to limit the spread of the pandemic, contamination by SARS-CoV-2 continues with the emergence of different variants such as Alpha, Beta, Delta, Gamma, Omega, and Omicron [6]. In response, various techniques and disinfectant agents have been employed to combat the pandemic [7, 8]. To understand the mechanism of the pandemic's spread, several models have been used, including statistical [9], mathematical [10–15], computational simulation [16–18], and numerical simulation [19–21]. The techniques of machine learning [22–25] and Big Data are also used [26–28]. The first and the most popular model is called the suspected, infected and recovered individuals model (SIR model) [29–32]. Several models based on the SIR model are reported in bibliography among them the SEIR model [33], SIRD model [34], etc.Scientists of different discipline, epidemiologists, biologists, physicists, chemists have adopted different approaches in connection with their specialty and knowledge. In fact, Mun and Geng [35] have proposed a mathematical model inspired by the mixed-order chemical reaction theory. By establishing an analogy between certain colloid system and the dynamic of virus infection, Tao et al. [36] have developed an approach to analyze and predict the temporary evolution of the pandemic. Nalosco et al. [37] have proposed a phenomenological COVID-19 model by establishing electrical-circuit model. In previous work [38], we showed that the sigmoidal-Boltzmann mathematical model is a tool that can be efficiently used to study the spread of COVID-19. Empirical laws between different parameters have been used to propose a modified sigmoidal-Boltzmann equation that describes the spread of the pandemic in 15 countries with 1 or 2 pandemic waves. We also focused on [39] using percolation theory to describe the cumulative number of infected people over time, and introduced several quantities such as pandemic percolation time and characteristic contamination frequency. Afterward, Pal et al. [40] present a model for the double-wave transmission of COVID-19 pandemics in Iceland using the double sigmoidal-Boltzmann equation (DSBE). The authors perform simulations to align the model to the cumulative number of COVID-19 infections for the entire country and examine the outcomes. Therefore, most studies have primarily investigated the changes in infection rates during one or two pandemic waves. However, given the emergence of new mutations and limited vaccine availability, COVID-19 has persisted for more than three years, leading to multiple waves of infection in many countries (3 or more). As a result, efforts have been made to understand the dynamics of the virus during these multiwave outbreaks. Notably, despite the complexity of modeling, few attempts have been made in this area by researchers such as the work of Cacciapaglia et al. [41] who discussed the multiwave pandemic dynamics and how it can be explained through the epidemic renormalization group (eRG) framework. The authors propose that understanding this time structure

a e-mail: gtarimoez@yahoo.fr (corresponding author)

Springer

is of paramount importance in designing effective prevention measures to tame the next wave of COVID-19. Xue et al. [42] used social awareness data to predict the evolution of multiwaves. They used a graph neural network to trace the COVID-19 spread. Otherwise, Shayak et al. [43] developed a model which correlates the reproduction number to the multiwaves spreading immunity. In addition, Chandra and Abdullah [44] have proposed a Bayesian protected-infected-recovered-dead multiwave model. Multiwave SIR-based models are also reported in the literature which can detect and model the waves of the disease and identify new waves [45, 46]. Grinchuk and Fisenko [47] have proposed a power-law multiwave model in order to describe the spread of the pandemic in a country non-uniform population density without quarantine. Despite the significance of these contributions, the probabilistic aspect has predominantly featured in the majority of the results, often leading to issues of convergence. A mathematical approach is therefore required to overcome these problems. In this study, we propose an extension of our previous work that was based on the sigmoidal growth of a pandemic wave. The approach involves considering successive pandemic waves as successive sigmoids. To achieve this, we explore several sigmoidal models from the literature to establish an equation for the modeling of successive waves. Furthermore, we propose interpreting pandemic waves as a succession of percolation phases. The theoretical developments are then applied to analyze the spread of the pandemic in four different countries during the time period between February 2020 and August 2022 in the second section of the paper.

2 Theoretical background

2.1 Sigmoidal models for one wave

2.1.1 The modified sigmoidal-Boltzmann model (MSBE)

The Boltzmann sigmoid model is commonly applied in the analysis of electrical percolation processes [48], viscosimetric percolation [49] and dielectic percolation [50, 51]. It is still used in several fields of materials science, such as phase transitions and chemorheology [52, 53]. In a previous study [39], we modeled the spread of COVID-19 in different countries that experienced a single pandemic wave using the Boltzmann sigmoid equation:

$$I(t) = I_{\max}\left[1 - \left\{1 + \exp(t - t_p)/\tau\right\}^{-1}\right] \tag{1}$$

where $I_{\max}$, t_p and τ, are, respectively, the final value of the infected person, corresponds to the pandemic peak and a time constant. We have shown also that the pandemic stabilizes when $I(t_\infty) = 0.99\, I_{\max}$. The infinite time, t_∞, can be determined according to Eq. (2).

$$t_\infty = 2.19\tau + t_p \tag{2}$$

The pandemic velocity deduced from Eq. (1) according to the following:

$$V_p(t) = \frac{\partial I}{\partial t} = \frac{I_{\max} e^{\frac{t-t_p}{\tau}}}{\tau\left(1 + e^{\frac{t-t_p}{\tau}}\right)^2} \tag{3}$$

Based on an analogy between the variation of electric conductivity in reverse micelles with temperature and the temporal evolution of cumulative infected individuals (I) over time, we also showed that the pandemic spread could be treated as a percolation phase [38]. In the present work, we examine the sigmoid dose–responsethe sigmoid dose–response, sigmoid Hill, and sigmoid logistic models and propose modified, novel equations to analyze the pandemic spread.

2.1.2 The modified sigmoid dose response equation (MSDRE)

The dose response model is widely used in the medical field due to its ability to evaluate the response of anticancer agents [54]. It is also used in toxicology and pharmacology [55]. The sigmoid dose response equation is given by the following:

$$y = A_1 + (A_2 - A_1)\left(1 + 10^{(x_0-x)h}\right)^{-1} \tag{4}$$

where A_1 and A_2, are, respectively, the lower and the higher values; x is independent variable; x_0 is the value of the x-axis midway between the bottom and the upper value of y value and h is the stiffness of the curve around x_0. So, a modified sigmoid dose response equation (MSDRE) is proposed:

$$I(t) = I_{\min} + (I_{\max} - I_{\min})\left(1 + 10^{\frac{t_p-t}{\tau}}\right)^{-1} \tag{5}$$

where I_{max} and I_{min}, are, respectively, the maximum and minimum infected persons, t_p and $\tau = 1/h$, are, respectively, the half of pandemic time and the pandemic relaxation constant. Therefore, we can propose the following equation:

$$I(t_p) = \frac{(I_{min} + I_{max})}{2} \qquad (6)$$

The epidemic state stabilizes when the number of infected cases I reaches almost the maximum number of infected cases $I(t_\infty)$ $= 0.99 I_{max}$ which corresponds to infinite time, t_∞ of pandemic spread. Taking into account that the pandemic begins with a single infected case, $I_0 = 1$, the t_∞ value for the first pandemic wave can be calculated from the following equation:

$$t_\infty = t_p + 2\tau \qquad (7)$$

By considering that $I_{max} << I_{min}$, the pandemic spread Eq. (5) according to the MSDRE takes the following form:

$$I(t) \approx I_{min} + I_{max}\left(1 + 10^{\frac{t_p - t}{\tau}}\right)^{-1} \qquad (8)$$

The pandemic velocity is deduced from the MSDRE equation:

$$V_p(t) = \frac{\partial I}{\partial t} = \frac{I_{max}}{\tau} \frac{\ln 10.10^{\frac{t_p - t}{\tau}}}{\left(1 + 10^{\frac{t_p - t}{\tau}}\right)^2} \qquad (9)$$

2.1.3 The modified sigmoid Hill equation (MSHE)

A.V. Hill first proposed the Hill equation to describe the equilibrium relationship between oxygen tension and hemoglobin saturation. It has also been used to predict the temporal variation of cytotoxicity [56]. Furthermore, the Hill model highlights its efficiency in the simulation of muscle dynamics [57] and the transpolar potential of the solar wind electric field [58]. The sigmoidal-Hill equation is given by the following:

$$y = A_1 + (A_2 - A_1)\left(1 + \left(\frac{k}{x}\right)^n\right)^{-1} \qquad (10)$$

where A_1, A_2, n and k, are, respectively, the initial value, the ultimate value, the Hill coefficient and the abscess of inflexion point. So, a modified sigmoidal Hill equation (MSHE) is proposed:

$$I(t) = I_{min} + (I_{max} - I_{min})\left(1 + \left(\frac{k}{t}\right)^n\right)^{-1} \approx I_{min} + I_{max}\left(1 + \left(\frac{k}{t}\right)^n\right)^{-1} \qquad (11)$$

The pandemic velocity is deduced from the MSHE:

$$V_p(t) = \frac{\partial I}{\partial t} = (I_{max} - I_{min})\frac{nk^n t^{n-1}}{(k^n + t^n)^2} \approx I_{max}\frac{nk^n t^{n-1}}{(k^n + t^n)^2} \qquad (12)$$

2.1.4 The modified sigmoidal logistic equation (MSLE)

Since the appearance of COVID-19, the logistic equation has been widely used in a variety of works [59, 60]. It has also long been regarded as one of the best equations for fitting sigmoidal growth, such as population evolution dynamics [61]. The sigmoidal logistic equation is given by the following:

$$y = A_1 + (A_2 - A_1)\left(1 + \left(\frac{x}{x_0}\right)^h\right)^{-1} \qquad (13)$$

where A_1, A_2, x_0 and h, are, respectively, the minimum y value, the maximum y value, the midway between the minimal and maximal response and the slope factor of the curve. So, a modified sigmoidal logistic equation (MSLE) is proposed:

$$I(t) = I_{min} + \frac{(I_{max} - I_{min})}{1 + \left(\frac{t}{t_p}\right)^h} \approx I_{min} + \frac{I_{max}}{1 + \left(\frac{t}{t_p}\right)^h} \qquad (14)$$

where I_{min}, I_{max}, t_p and h, are, respectively, the minimum value of infected persons, the maximum value of infected person, the half pandemic time and the slope factor of the curve.

So, the pandemic velocity is deduced from the MSLE:

$$V_P(t) = \frac{\partial I}{\partial t} = \frac{I_{max}}{\left(1 + \left(\frac{t}{t_p}\right)^h\right)^2}\left(\frac{t}{t_p}\left(\frac{t}{t_p}\right)^{h-1}\right) \qquad (15)$$

2.2 Sigmoidal models for one two waves

2.2.1 The double sigmoidal-Boltzmann equation (DSBE)

In our previous work [39], we have succeed in modeling the spread of the virus in countries having experienced two pandemic waves by a double sigmoid Boltzmann equation (DSBE) of the following form:

$$I(t) = I_{\max} \left(\frac{p}{1 + \exp\left(\frac{t - t_{p1}}{\tau_1}\right)} + \frac{1 - p}{1 + \exp\left(\frac{t - t_{p2}}{\tau_2}\right)} \right) \tag{16}$$

where $I_{\max}$, p, $1 - p$, are, respectively, the maximum values taken by I, the fraction of the first curve, $1 - p$ is the fraction of the second wave 2. τ_1, τ_2, t_{p1} and t_{p2} are the time constant interval of the wave 1, the time constant of the wave 2, the pandemic peak of the wave 1 and the pandemic peak of the wave 2. In this case, the spread velocity for two waves is given by the following:

$$V_p(t) = I_{\max} \left(\frac{p e^{\left(\frac{t - t_{p1}}{\tau_1}\right)}}{\tau_1 \left(1 + e^{\left(\frac{t - t_{p1}}{\tau_1}\right)}\right)^2} + \frac{(1 - p) e^{\left(\frac{t - t_{p2}}{\tau_2}\right)}}{\tau_2 \left(1 + e^{\left(\frac{t - t_{p2}}{\tau_2}\right)}\right)^2} \right) \tag{17}$$

2.2.2 The double sigmoidal dose response equation (DSDE)

According to our precedent developments, we propose a double sigmoidal dose response equation to analyze the pandemic spread in two waves:

$$I(t) \approx I_{\min} + I_{\max} \left(\frac{p}{\left(1 + 10^{\left(\frac{t_{p1} - t}{\tau_1}\right)}\right)} + \frac{1 - p}{\left(1 + 10^{\left(\frac{t_{p2} - t}{\tau_2}\right)}\right)} \right) \tag{18}$$

where $I_{\min}$, $I_{\max}$, p, $1 - p$, are, respectively, the minimum value taken by I, the maximum values taken by I, the fraction of the first curve, the fraction of the second wave 2. τ_1, τ_2, t_{p1} and t_{p2} are the pandemic relaxation constant of the first wave, the pandemic relaxation constant of the second wave, the pandemic peak of the wave 1 and the pandemic peak of the wave 2. In this case, the spread velocity for two waves is given by the following:

$$V_p(t) \approx \ln 10 I_{\max} \left(\frac{\frac{p}{\tau_1} 10^{\left(\frac{t_{p1} - t}{\tau_1}\right)}}{\left(1 + 10^{\left(\frac{t_{p1} - t}{\tau_1}\right)}\right)} + \frac{\frac{1 - p}{\tau_2} 10^{\left(\frac{t_{p2} - t}{\tau_2}\right)}}{\left(1 + 10^{\left(\frac{t_{p2} - t}{\tau_2}\right)}\right)} \right) \tag{19}$$

2.2.3 The double sigmoidal Hill equation (DSHE)

According to our precedent developments, we propose a double sigmoidal Hill equation to analyze the pandemic spread in two waves:

$$I(t) \approx I_{\min} + I_{\max} \left(\frac{p}{1 + \left(\frac{k_1}{t}\right)^{n_1}} + \frac{1 - p}{1 + \left(\frac{k_1}{t}\right)^{n_2}} \right) \tag{20}$$

where $I_{\min}$, $I_{\max}$, p, $1 - p$, are, respectively, the minimum value taken by I, the maximum values taken by I, the fraction of the first curve, the fraction of the second wave 2. k_1, k_2, n_1 and n_2, are, respectively, the Hill coefficients of the waves 1 and 2, the abscess of inflexion points of waves 1 and 2. In this case, the spread velocity for two waves is given by the following:

$$V_p(t) \approx I_{\max} \left(\frac{p n_1 k_1^n}{t^{n_1 + 1} \left(1 + \left(\frac{k_1}{t}\right)^{n_1}\right)^2} + \frac{(1 - p) n_1 k_2^n}{t^{n_2 + 1} \left(1 + \left(\frac{k_1}{t}\right)^{n_2}\right)^2} \right) \tag{21}$$

2.2.4 The double sigmoidal logistic equation (DSLE)

The double sigmoidal logistic equation (DSLE) is given according to the following:

$$I(t) \approx I_{\min} + I_{\max} \left(\frac{p}{1 + \left(\frac{t}{t_{p1}}\right)^{h_1}} + \frac{1-p}{1 + \left(\frac{t}{t_{p2}}\right)^{h_2}} \right) \tag{22}$$

where $I_{\min}$, $I_{\max}$, p, $1-p$, are, respectively, the minimum value taken by I, the maximum values taken by I, the fraction of the first wave, the fraction of the second wave 2. h_1, h_2, t_{01} and t_{02}, are, respectively, the slope factor of the wave 1, the slope factor of the wave 2, the half pandemic time of the first wave and the half pandemic time of the second wave. The pandemic velocity can be deduced from Eq. (22), according to the following:

$$V_p(t) = \frac{\partial I}{\partial t} = I_{\max} \left(p \frac{\frac{h_1}{t_{p1}} \left(\frac{t}{t_{p1}}\right)^{h_1-1}}{\left(1 + \left(\frac{t}{t_{p1}}\right)^{h_1}\right)^2} + (1-p) \frac{\frac{h_2}{t_{p2}} \left(\frac{t}{t_{p2}}\right)^{h_2-1}}{\left(1 + \left(\frac{t}{t_{p2}}\right)^{h_2}\right)^2} \right) \tag{23}$$

2.3 Sigmoidal models for N waves (N ≥ 3)

2.3.1 The N-sigmoidal-Boltzmann equation (NSBE)

The reported result for one and two waves, as given in Eqs. (1) and (16), can be extended to N waves according to the following:

$$I_N(t) = I_{\max} \sum_{i=1}^{N} p_i \left(1 + \exp\left(\frac{t - t_{pi}}{\tau_i}\right) \right)^{-1} \tag{24}$$

where p_i, t_{pi} and τ_i, are, respectively, the fraction of wave i with respect to the total number of waves N, the percolation time, the time constant of the wave i. $I_{\max}$, is the maximum value of the cumulative infected persons. The pandemic velocity over N waves is given as follows:

$$V_p(t) = I_{\max} \sum_{i=1}^{N} \left[\frac{p_i e^{\left(\frac{t-t_{pi}}{\tau_i}\right)}}{\tau_i \left(1 + e^{\left(\frac{t-t_{pi}}{\tau_i}\right)}\right)^2} \right] \tag{25}$$

2.3.2 The N-sigmoidal dose response equation (NSDRE)

The sigmoidal dose response equation can be extended to study the pandemic spread over N waves, according to our precedent developments, as given in Eqs. (5) and (18). So, the number of cumulative infected persons is given by Eq. (26).

$$I(t) \approx I_{\min} + I_{\max} \sum_{i=1}^{N} \left[\frac{p_i}{\left(1 + 10^{\left(\frac{t_{pi}-1}{\tau_i}\right)}\right)} \right] \tag{26}$$

where $I_{\min}$, $I_{\max}$, p_i and τ_i, are, respectively, the minimum value taken by I, the maximum values taken by I, the pandemic peak of the wave i and the pandemic relaxation constant of the wave i. The pandemic velocity over N waves is given as follows:

$$V_p(t) \approx \ln 10 \, I_{\max} \sum_{i=1}^{N} \left[\frac{p_i 10^{\left(\frac{t_{pi}-1}{\tau_i}\right)}}{\tau_i \left(1 + 10^{\left(\frac{t_{pi}-1}{\tau_i}\right)}\right)^2} \right] \tag{27}$$

2.3.3 The N-sigmoidal Hill equation (NSHE)

The sigmoidal Hill equation can be extended to study the pandemic spread over N waves, according to our precedent developments, as given in Eqs. (11) and (20). So, the number of cumulative infected persons is given by Eq. (28).

$$I(t) \approx I_{\min} + I_{\max} \sum_{i=1}^{N} \left[\frac{p_i}{1 + \left(\frac{k_i}{t}\right)^{n_i}} \right] \tag{28}$$
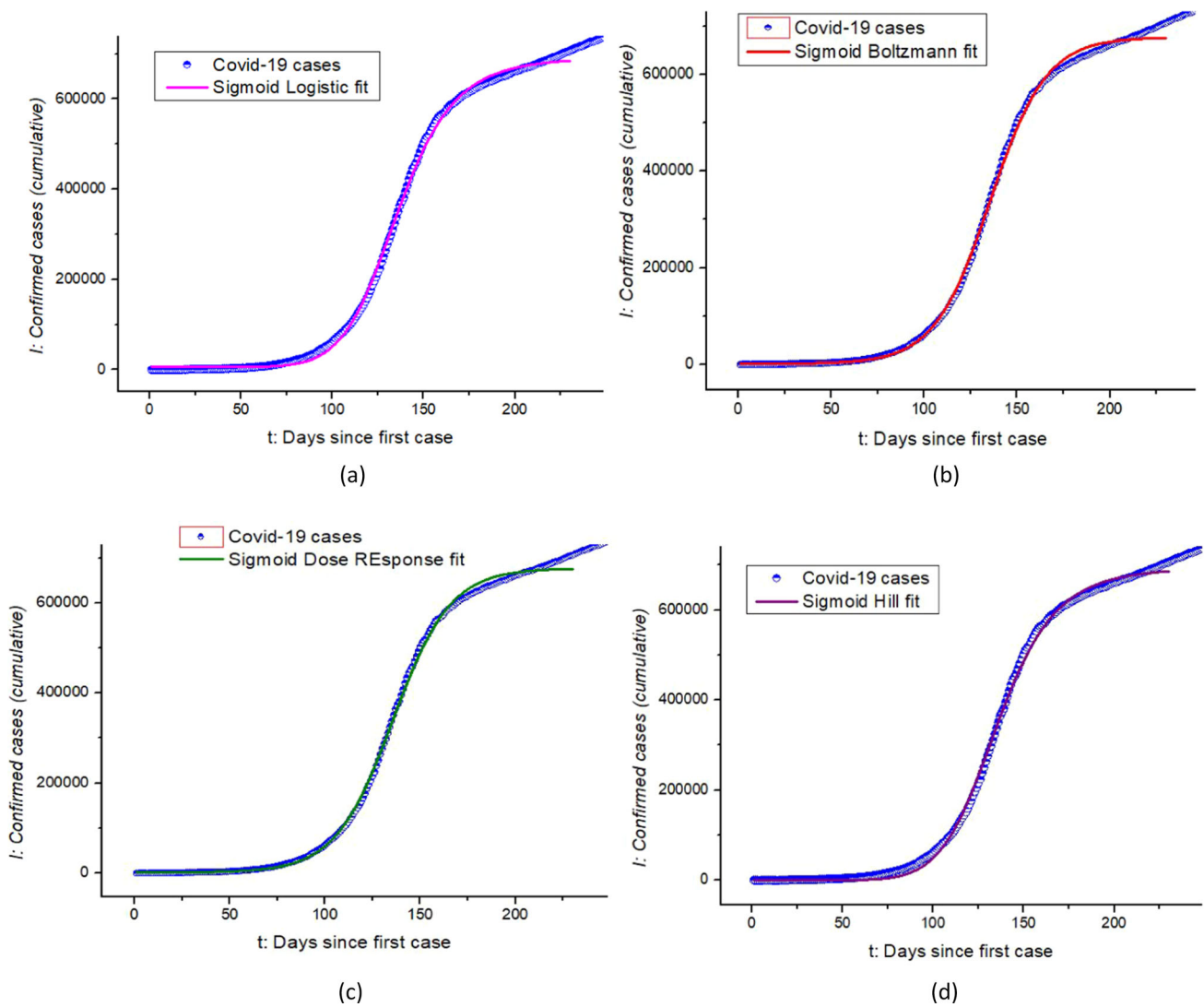
Fig. 1 The variation of the Number of infected cases (I) as a function of time (t) of the first Covid-19 wave in south africa, fitted by the different sigmoid models: **a** logistic model, **b** sigmoid Boltzmann model, **c** dose response model **d** Hill model

where I_{min}, I_{max}, p_i, are, respectively, the minimum value taken by I, the maximum values taken by I, the fraction of the pandemic wave,i. k_i and n_i, are, respectively, the Hill coefficients of the wave i and the abscess of inflexion points of waves i. The spread velocity for two waves is given by the following:

$$V_p(t) \approx I_{max} \sum_{i=1}^{N} \left[\frac{p_i n_i k_i^{n_i}}{t^{n_i+1} \left(1 + \left(\frac{k_i}{t}\right)^{n_i}\right)^2} \right] \tag{29}$$

2.3.4 The N-sigmoidal logistic equation (NSLE)

The sigmoidal logistic equation can be extended to study the pandemic spread over N waves, according to our precedent developments, as given in Eqs. (14) and (22). So, the number of cumulative infected persons is given by Eq. (30).

$$I(t) \approx I_{min} + I_{max} \sum_{i=1}^{N} \left[\frac{p_i}{1 + \left(\frac{t}{t_{pi}}\right)^{h_i}} \right] \tag{30}$$

Table 1 Pandemic parameters of the first COVID-19 wave in South Africa modeled by the 4 sigmoidal equations (Eqs. (1, 7, 8, 11, 14))

Model	I_{min}/persons	I_{max}/persons	n	t_p/days	τ	Adj. R square
Modified sigmoidal-Boltzmann equation (MSBE)	1288	676,870	–	135.580	15.130	0.999
Modified sigmoidal dose response equation (MSDRE)	1288	676,870	–	135.580	0.028	0.999
Modified sigmoidal-Hill equation (MSHE)	1540	693,874	8.454	135.577	–	0.998
Modified sigmoidal logistic equation (MSLE)	6207	691,502	–	135.847	8.689	0.999

Table 2 Statistic parameters of the two COVID-19 waves in UK ajusted by the 4 sigmoidal equations (Eqs. 15, 17, 19, 21)

Model	Reduced Chi-Sqr	Adj. R-square	Fit status
Double sigmoidal-Boltzmann equation (DSBE)	$1.816.10^8$	0.999	Succeeded (100)
Double sigmoidal Hill equation (DSHE)	$6.641.10^{13}$	-0.072	Failed
Double sigmoidal dose response equation (DSDRE)	$1.942.10^8$	0.999	Succeeded (100)
Double sigmoidal logistic equation (DSLE)	$1.666.10^{14}$	0.280	Failed

where I_{min}, I_{max} and p_i,are, respectively, the minimum value taken by I, the maximum values taken by I, the fraction of the wave, i. h_i and t_{pi}, are, respectively, the slope factor of the wave i and the half pandemic time of wave, i. The pandemic velocity can be deduced from Eq. (31), according to the following:

$$V_p(t) = \frac{\partial I}{\partial I} = I_{max} \sum_{i=1}^{N} \left[p_i \frac{\frac{h_i}{t_{pi}} \left(\frac{t}{t_{pi}} \right)^{h_i - 1}}{\left(1 + \left(\frac{t}{t_{pi}} \right)^{h_i} \right)^2} \right] \tag{31}$$

3 Case study

3.1 Analysis of pandemic spread over one wave

We adjusted the curves of variation of the number of confirmed cases (cumulated) in South Africa during the first pandemic wave based on the four models described below. The results shown in Fig. 1 show a perfect fit by the four equations. The fit parameters for the four equations are reported in Table 1.

Table 1 demonstrates that the percolation characteristics of the pandemic for the Boltzmann sigmoid and dose response models are comparable, with similar minimum and maximum cumulative infected individuals (I_{min} and I_{max}) and percolation time. However, the logistic model stands out with a significantly larger initial number of cases (I_{min}) compared to the other models and has a comparable number of total cases (I_{max}) to Hill's model at the end of a wave.

3.2 Analysis of pandemic spread over multiwaves

In our study, we considered the cases of countries with different number of waves ($N = 2$ for the UK, $N = 3$ for Zambia, $N = 4$ for Brazil, and $N = 5$ for South Africa) based on general spread equations for multiple successive waves. All cumulative infected individuals data was obtained from the COVID-19 Dashboard by John Hopkins University [62].

3.2.1 N = 2

The data for the case of the two-wave spread (the case of UK) were adjusted using Eqs. (16, 18, 20, and 22) of different models. The results showed that only the fit converged for Eqs. 16 and 18 (Boltzmann sigmoid and dose response models). For the other two models (logistic and Hill), the adjusted correlation coefficient (Adj. R-square) values indicated that the fit was not achievable (Table 2).

3.2.2 N ≥ 3

The data for the case of countries with $N > 2$, Zambia, Brazil, and South Africa was adjusted using Eqs. (24) and (26), dose response and Boltzmann sigmoid models. The results showed that only the dose response model fitted successfully (Figs. 2, 3, 4, 5 and

Fig. 2 Variation of the number of cumulative cases over time in the UK fitted by N-generalized spread equation, $N = 2$
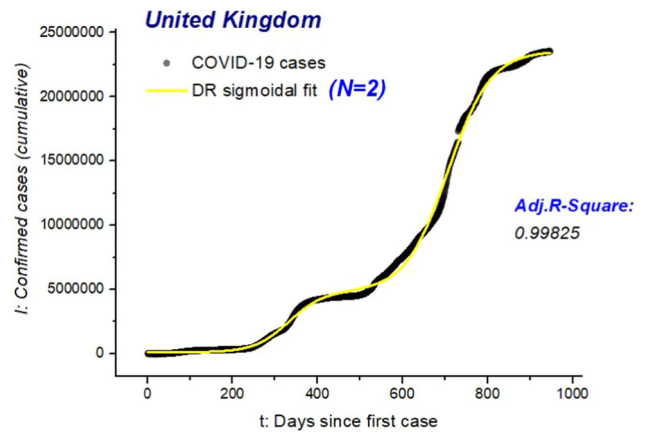

Fig. 3 Variation of the number of cumulative cases over time in Zambia fitted by N-generalized spread equation, $N = 3$
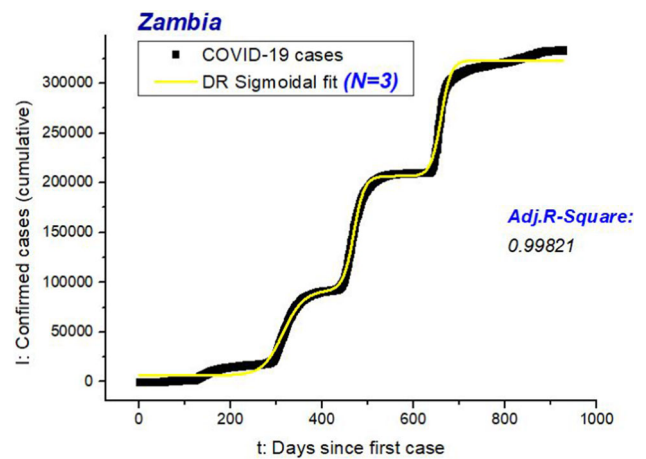

Fig. 4 Variation of the number of cumulative cases over time in Brazil fitted by N-generalized spread equation, $N = 4$
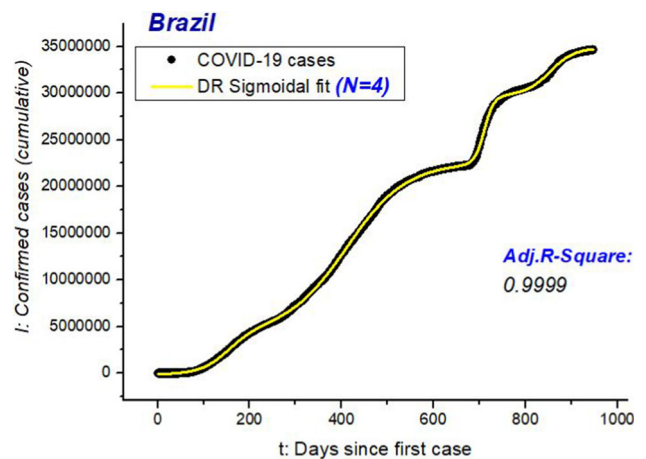

Table 3). Hence, we can conclude that the general dose response equation (Eq. 23) is the most appropriate equation for analyzing multiwave COVID-19 spread data.

The explicit expressions of the spread equations in the 4 studied countries have been presented in Eqs. (32)–(35):

3.2.3 UK (N = 2)

$$I_2(t) = 109421.934 + 2.357.10^7 \left[\frac{0.200}{\left(1 + 10^{(332-t)0.01}\right)} + \frac{0.800}{\left(1 + 10^{(706-t)0.007}\right)^{-1}} \right] \tag{32}$$

Fig. 5 Variation of the number of cumulative cases over time in South Africa fitted by N-generalized spread equation, $N = 5$
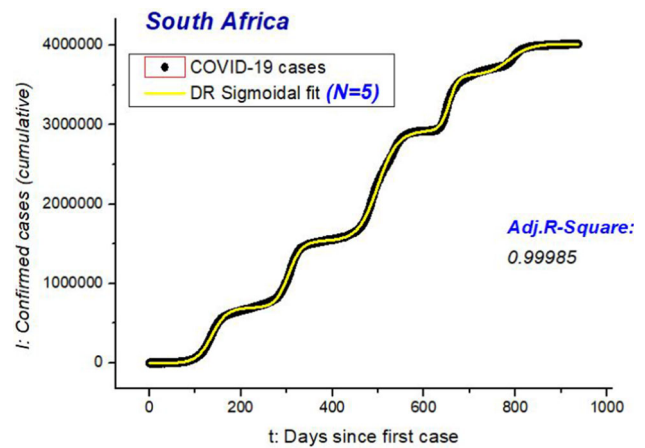

Table 3 Statistic parameters of the 5 COVID-19 waves in South Africa adjusted by the 2 sigmoidal equations (Eqs. (23, 25))

	Reduced Chi-Sqr	Adj. R-square	Fit status
N-sigmoidal-Boltzmann equation (NSBE)	$1.280.10^{14}$	0.027	Failed
N-sigmoidal dose response equation (NSDRE)	$2.281.10^{11}$	0.997	Succeeded (100)

3.2.4 Zambia (N = 3)

$$I_3(t) = 6390.804 + 372055.186\left[\frac{0.234}{1 + 10^{(315.160-t)0.019}} + \frac{0.313}{1 + 10^{(469.382-t)0.037}} + \frac{0.318}{1 + 10^{(659.856-t)0.039}}\right] \tag{33}$$

3.2.5 Brazil (N = 4)

$$I_4(t) = 160828.817 + 3.975.10^7\left[\frac{0.114}{1 + 10^{(152.873-t)0.014}} + \frac{0.455}{1 + 10^{(411.206-t)0.006}}\right.$$
$$\left. + \frac{0.125}{1 + 10^{(710.577-t)0.016}} + \frac{0.181}{1 + 10^{(853.975-t)0.041}}\right] \tag{34}$$

3.2.6 South Africa (N = 5)

$$I_5(t) = 1623.592 + 4.102.10^6\left[\frac{0.170}{1 + 10^{(136.818-t)0.026}} + \frac{0.204}{1 + 10^{(304.385-t)0.030}}\right.$$
$$+ \frac{0.337}{1 + 10^{(499.514-t)0.020}} + \frac{0.170}{1 + 10^{(655.295-t)0.044}}$$
$$\left. + \frac{0.095}{1 + 10^{(786.989-t)0.019}}\right] \tag{35}$$

The different pandemic parameters (fraction of each wave, pandemic peaks, final number of cases, pandemic relaxation…) related to each country are presented in Table 4.

The reliability of the model can be estimated by comparing the final number of infected cases at the end of the study period, I_{max} as predicted by the proposed equation (Eq. 26), with the number recorded in the official database for each country [5, 62]. For this purpose, a relative deviation was measured by the following equation:

$$\varepsilon = \left|\frac{I_{max,\,ref} - I_{max}}{I_{max,\,ref}}\right| \tag{36}$$

where $I_{max,\,ref}$ is the maximum number of cases reported in official Data. The results presented in Table 5 indicate that the proposed equation has demonstrated a good level of accuracy in predicting values, with deviations ranging from 0.2% to 15%. This suggests that the NSDRE equation (Eq. 25) is a effective tool for analyzing the propagation curves of COVID-19 (Figs. 6, 7).

Otherwise, in the context of the COVID-19 pandemic, an important epidemiological parameter for countries experiencing multiple waves is the relative intensity of each wave. The present study considers the fraction of the sigmoid of the propagation curve, specifically represented by the p_i parameter in Eq. (26), to quantify the magnitude of each pandemic wave. The analysis included a comparison of the different waves across four countries ($N = 2…5$), which is illustrated in Fig. 8a. The findings indicate that the second wave was the most severe across all four countries, followed by the third wave. Conversely, a decrease in magnitude

Table 4 Pandemic parameters of a multiwaves Covid-19 spread determined using Eq. 25: Case studies include South Africa ($N = 5$), Brazil ($N = 4$), Zambia ($N = 3$) and the UK ($N = 2$)

Pandemic characteristics	$N = 2$ UK	$N = 3$ Zambia	$N = 4$ Brazil	$N = 5$ South Africa
Wave fraction				
p1	0.200	0.234	0.114	0.170
p2	0.800	0.313	0.455	0.204
p3		0.318	0.125	0.337
p4			0.181	0.170
p5				0.095
Slope factor				
h_1	0.010	0.019	0.014	0.026
h_2	0.007	0.037	0.006	0.030
h_3		0.039	0.016	0.020
h_4			0.041	0.044
h_5				0.019
Wave pic				
t_{p1}	332.000	315.160	152.873	136.818
t_{p2}	706.670	469.382	411.206	304.385
t_{p3}		659.856	710.577	499.514
t_{p4}			853.975	655.295
t_{p5}				786.989
Maximum cases: I_{max}	$2.357.10^7$	372,055.186	$3.975.10^7$	$4.102.10^6$
Wave relaxation				
τ_1	100	52.631	71.428	38.461
τ_2	142.857	27.027	166.666	33.333
τ_3		25.641	62.500	50.000
τ_4			24.390	22.727
τ_5				52.631

Table 5 Relative deviation between the official maximum number of infected cases in the end of multiwaves spread $I_{max, ref}$ and the values predicted by Eq. (26) I_{max}

Country	$I_{max, ref}$	I_{max}	$\varepsilon(\%)$
UK	$2.535.10^7$	$2.357.10^7$	0.208
Brazil	$3.431.10^7$	$3.975.10^7$	15.310
South Africa	$4.011.10^6$	$4.102.10^6$	2.218
Zambia	332,822	372,055.186	11.787

was observed for the fourth and fifth waves. It is notable that the fourth and fifth waves reached their pandemic peaks approximately 700 days (Table 4) after the onset of the pandemic, which means that this observation could potentially be attributed to the emergence of systemic immunity, which may be attributable to vaccination efforts. In addition, Fig. 8b displays the relative fluctuation in the number of COVID-19 cases in proportion to each country's population. Notably, the data reveals that the UK = 2) has been the country most severely impacted by the pandemic, despite having fewer waves than other countries, such as South Africa = 5), which experienced multiple waves but did not have the highest number of cases overall. This observation highlights that the number of pandemic waves is not always a reliable indicator of the most affected country.

3.3 Multiphasic pandemic percolation and wave relaxation

First introduced by condensed matter physicists to model flow in porous media [63], percolation theory has been widely used to describe the evolutionary dynamics of epidemics. A large-scale connectivity is formed from local connections that develop in a probabilistic manner. Since the emergence of the Covid-19 coronavirus, several works have used percolation to develop predictive models of a mathematical and statistical nature [64].

Typically, the percolation phase is analyzed using two-dimensional networks made up of nodes. At the beginning, nodes are randomly connected to each other with a probability that varies between 0 and 1. The fraction of connected nodes is commonly referred to as ρ. When a large-scale connectivity is established between the nodes, it is referred to as the appearance of a percolating network. The fraction at which this connectivity appears is known as the percolation point, denoted ρ_c. A pandemic wave is analogous

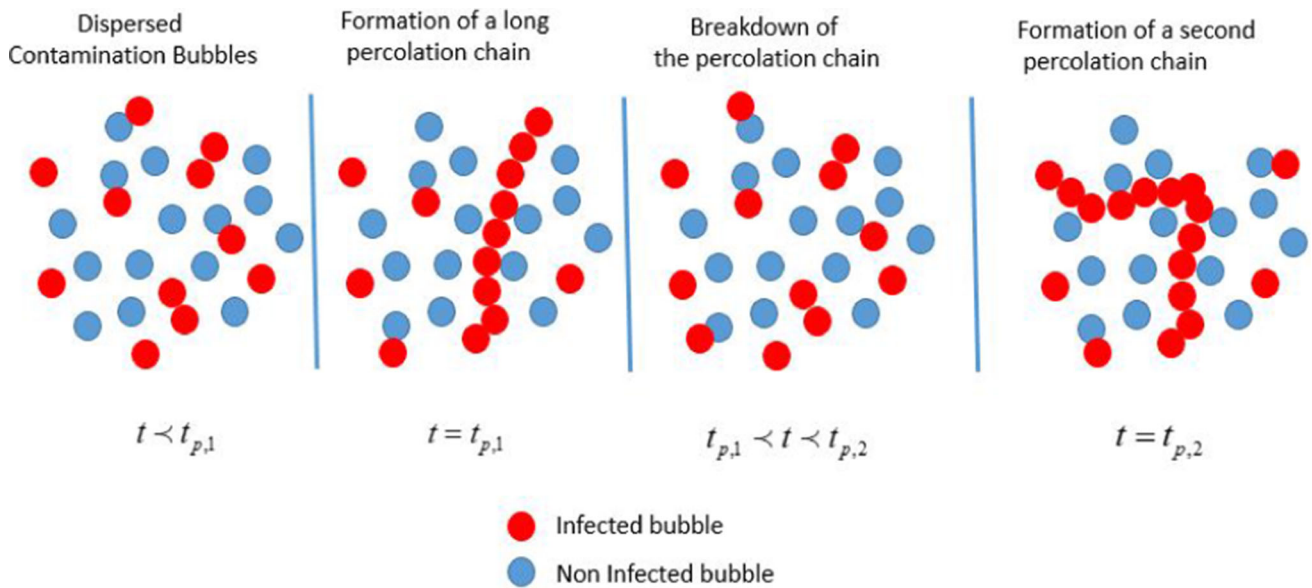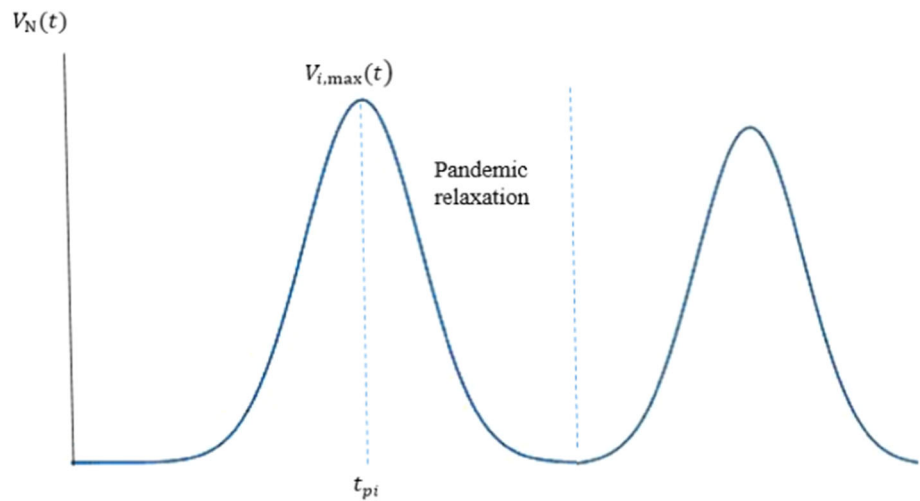**Fig. 6** Schematic representation of the Formation and the destruction of long chain of infection during 2 successive wave

Fig. 7 Schematic representation of the pandemic relaxation period during 2 successive wave

to the appearance of local contamination bubbles [64] the creation of a percolating network constitutes a bridge of large dimension for the circulation of a virus, hence the increase in the speed of propagation of the virus and the explosion in the number of infected cases. The critical percolation point ρ_C is therefore linked to the day of the pandemic peak t_p. After the peak of a pandemic wave, the speed at which the virus spreads decreases exponentially. This decrease can therefore be attributed to a break in the percolating chain. Danone et al. [64] have proceeded by measuring the proportion of links that need to be removed to break up the giant network. As a result, as the fraction of connected bubbles ρ decreases, the fraction of unconnected bubbles $1 - \rho$ increases. We can therefore call this process epidemic relaxation. For a multiwave propagation of an epidemic, the successive epidemic waves are a succession of percolation phases separated by periods of epidemic relaxation where the chains of infection are broken (Fig. 6).

The velocity equation (Eq. 27) therefore allowed us to discern this exponential decrease after each pandemic pic, for $t > t_{pi}$ above each wave i, where τ_i represents an epidemic relaxation constant, which corresponds to wave i. This constant may reflect the effectiveness of the barrier measures taken during each wave to break the chains of contamination (Fig. 7). The greater τ_i the slower the relaxation, so the measures taken are not effective enough. Low values of τ_i reflect the reliability of the measures taken to slow the spread. Data on variations in different spread velocity was fitted using Eq. (27). The results of a successful fit highlighted a good qualitative agreement (Figs. 9, 10, 11 and 12). However, from a quantitative point of view, the results showed low deviation, especially for the values of maximum spread velocity during each wave.
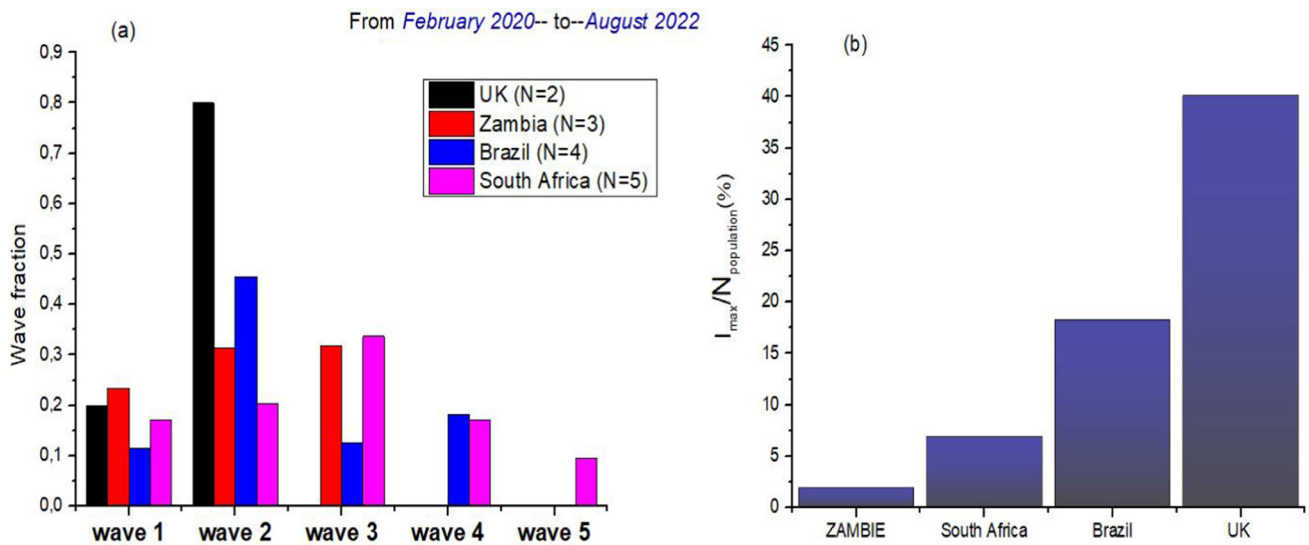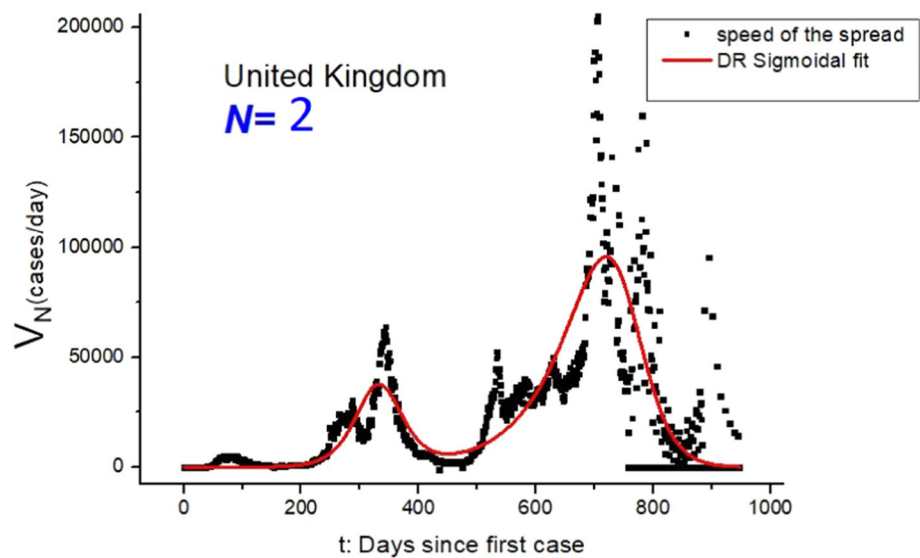
Fig. 8 a Intensities of different waves of COVID-19, for multiwave spread in 4 countries (UK, Zambia, South Africa, Brazil). **b** Overall infection rate relative to each country's population after multiwaves of COVID-19

Fig. 9 Variation of the number of cumulative cases over time in the UK fitted by N-generalized spread equation, $N = 2$

4 Conclusion

The present study's principal novelty can be pointed out in 2 points: Firstly, we have developed a general sigmoidal equation to model the transmission of Covid-19 across multiple waves. Secondly, we have interpreted the successive pandemic waves as a sequence of percolation and relaxation phenomena. These two points were derived from followings primary observations that have been made:

- Among the four sigmoidal models, the dose response model is considered the most appropriate for analyzing N pandemic waves.
- N-general equations for pandemic spread and the speed of virus spread were developed, and these equations successfully fit the data.
- The general N equation was adjusted for each country analyzed based on the number of waves observed over a three-year period ($N = 2$ in UK, $N = 3$ in Zambia, $N = 4$ in Brazil, $N = 5$ in South Africa).
- From a phenomenological perspective, successive waves were described as multiple percolation phases.
- The period between two successive phases was characterized as a period of pandemic relaxation, with relaxation constants reflecting the effectiveness of barrier measures.

In addition to statistical and numerical models, the sigmoid mathematical model has demonstrated efficacy in analyzing Covid-19 spread curves. Its significance lies in its association with the phenomenological aspect of spread represented by pandemic percolation. Therefore, the introduction of a general equation that incorporates various epidemiological parameters, including the pandemic peak,

Fig. 10 Variation of the number of cumulative cases over time in Zambia fitted by N-generalized spread equation, $N = 3$
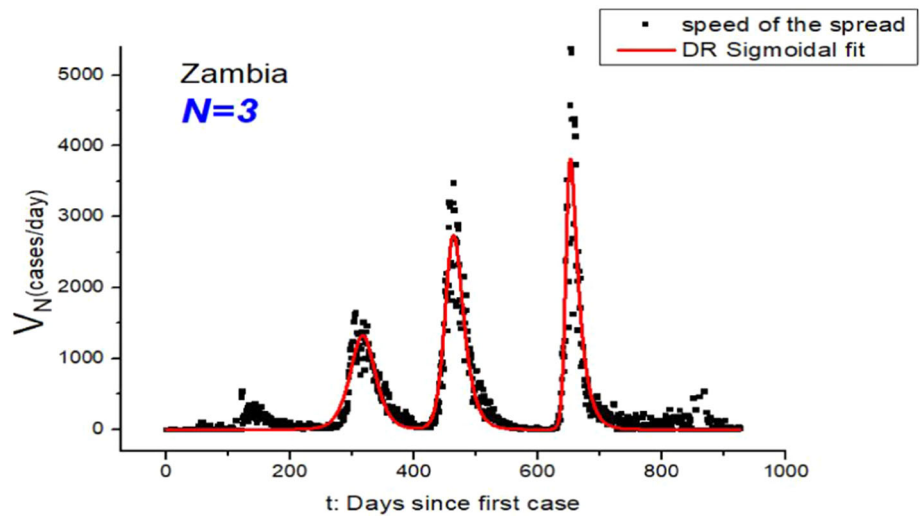

Fig. 11 Variation of the number of cumulative cases over time in Brazil fitted by N-generalized spread equation, $N = 4$
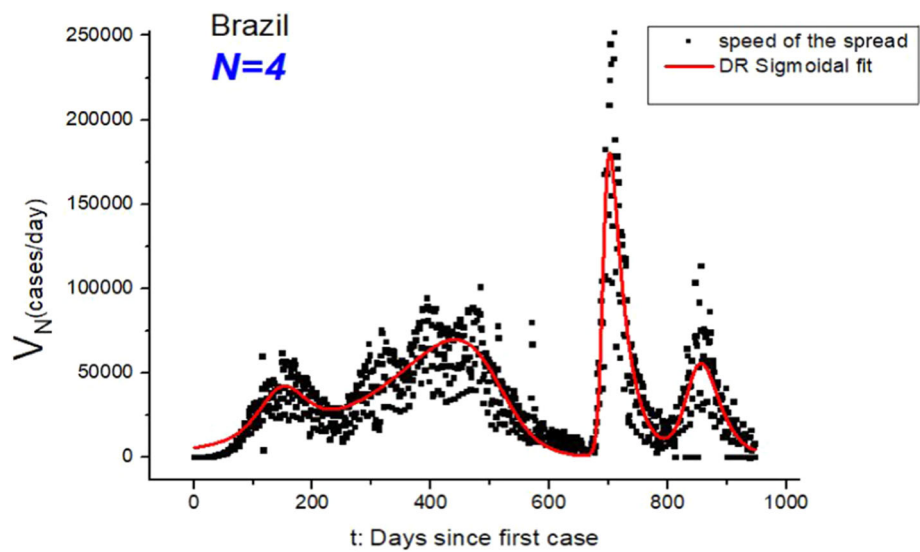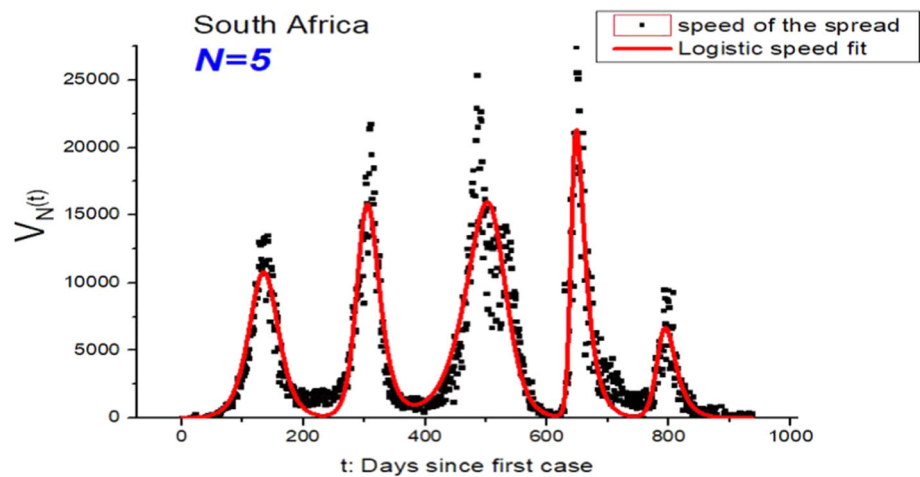

Fig. 12 Variation of the number of cumulative cases over time in South Africa fitted by N-generalized spread equation, $N = 5$

directly associated with the critical point of percolation, could be of immense value. This equation would not only facilitate the study of Covid-19 spread dynamics but also enable the extension of the analysis to other types of pandemics.

Data Availability Statement This manuscript has associated data in a data repository. [Authors' comment: The datasets analyzed during the current study are available in the Johns Hopkins Coronavirus Resource Center, https://coronavirus.jhu.edu/map.html].

Declarations

Conflict of interest The authors declare that they have no known competing financial interests or personal relationships that could have appeared to influence the work reported in this paper.

References

1. J. Abraham, C. Turville, K. Dowling, S. Florentine, Int. J. Environ. Res. Public Health **18**, 9086 (2021)
2. H. Bherwani, A. Gupta, S. Anjum, A. Anshul, R. Kumar, Npj Clim. Atmos. Sci. **3**, 1 (2020)
3. A. Singh, M. Arquam, Phys. A Stat. Mech. Appl. **592**, 126774 (2022)
4. A. M. Ibrahim, M. Mohammed Eid, N. N. Mostafa, N. E. H. Mohamed Bishady, S. H. Elghalban, Intell. Lead. Emerg. Sci. Conf. NILES 2020 612 (2020)
5. https://www.worldometers.info/coronavirus
6. https://www.contagionlive.com/view/variety-variants-covid-19
7. Y.-L. Cheng, C.-Y. Lee, Y.-L. Huang, C.A. Buckner, R.M. Lafrenie, J.A. Dénommée, J.M. Caswell, D.A. Want, G.G. Gan, Y.C. Leong, P.C. Bee, E. Chin, A.K.H. Teh, S. Picco, L. Villegas, F. Tonelli, M. Merlo, J. Rigau, D. Diaz, M. Masuelli, S. Korrapati, P. Kurra, S. Puttugunta, S. Picco, L. Villegas, F. Tonelli, M. Merlo, J. Rigau, D. Diaz, M. Masuelli, M. Tascilar, F.A. de Jong, J. Verweij, R.H.J. Mathijssen, INTECH **11**, 13 (2016)
8. L. Aleya, W. Gu, S. Howard, Environ. Sci. Pollut. Res. **28**, 40308 (2021)
9. S.K. Yadav, Y. Akhter, Front. Public Heal. **9**, 1 (2021)
10. K. Logeswari, C. Ravichandran, K. S. Nisar, Numer. Methods Partial Differ. Equ. 1 (2020).
11. M. Bachar, M.A. Khamsi, M. Bounkhel, Adv. Differ. Equations **2021**, 1–18 (2021)
12. P. Riyapan, S. E. Shuaib, A. Intarasit, **2021**, (2021).
13. N. Parolini, L. Dede', P. F. Antonietti, G. Ardenghi, A. Manzoni, E. Miglio, A. Pugliese, M. Verani, A. Quarteroni, Proc. R. Soc. A Math. Phys. Eng. Sci. **477**, (2021).
14. A.K. Sinha, N. Namdev, P. Shende, Netw. Model. Anal. Heal. Informatics Bioinforma. **11**, 1 (2022)
15. S.H.A. Khoshnaw, R.H. Salih, S. Sulaimany, Math. Model. Nat. Phenom. **15**, 33 (2020)
16. C. Balsa, I. Lopes, T. Guarda, J. Rufino, Comput. Math. Organ. Theory (2021).
17. C. Ohajunwa, K. Kumar, P. Seshaiyer, Comput. Math. Biophys. **8**, 216 (2020)
18. S.H.A. Khoshnaw, A.S. Mohammed, AIMS Bioeng. **9**, 239 (2022)
19. A.A. Khan, R. Amin, S. Ullah, W. Sumelka, M. Altanji, Alexandria Eng. J. **61**(5083), 14 (2022)
20. Alalyani, S. Saber, Int. J. Nonlinear Sci. Numer. Simul. (2022).
21. M. Rafiq, A.R. Nizami, D. Baleanu, N. Ahmad, Alexandria Eng. J. **62**, 75 (2023)
22. M. Pavlyutin, M. Samoyavcheva, R. Kochkarov, E. Pleshakova, S. Korchagin, T. Gataullin, P. Nikitin, M. Hidirova, Mathematics **10**, 1 (2022)
23. S. S. Arun, G. N. Iyer, Proc. Int. Conf. Intell. Comput. Control Syst. ICICCS 2020 1222 (2020).
24. N. S. Punn, S. K. Sonbhadra, S. Agarwal, MedRxiv **1** (2020).
25. M.A. Lmater, M. Eddabbah, T. Elmoussaoui, S. Boussaa, J. Infect. Public Health **14**, 468 (2021)
26. F. Villanustre, A. Chala, R. Dev, L. Xu, J. S. LexisNexis, B. Furht, T. Khoshgoftaar, J. Big Data **8**, (2021).
27. S.J. Alsunaidi, A.M. Almuhaideb, N.M. Ibrahim, F.S. Shaikh, K.S. Alqudaihi, F.A. Alhaidari, I.U. Khan, N. Aslam, M.S. Alshahrani, Sensors **21**, 2282 (2021)
28. T. Alamo, D.G. Reina, P. Millán Gata, V.M. Preciado, G. Giordano, Annu. Rev. Control **52**, 448 (2021)
29. E. Kenah, J.M. Robins, J. Theor. Biol. **249**, 706 (2007)
30. E. Kenah, J.M. Robins, Phys. Rev. E Stat. Nonlinear Soft Matter. Phys. **76**, 1 (2007)
31. S. Cauchemez, N.M. Ferguson, J.R. Soc, Interface **5**, 885 (2008)
32. Y. Tao, Phys. Rev. E **102**, 32136 (2020)
33. M.H.A. Biswas, L.T. Paiva, M. De Pinho, Math. Biosci. Eng. **11**, 761 (2014)
34. M. Matadi, (2014).
35. E.Y. Mun, F. Geng, PLoS ONE **16**, 1 (2021)
36. A. El Aferni, M. Guettari, T. Tajouri, Environ. Sci. Pollut. Res. **28**, 40400 (2021)
37. M. Guettari, A. El Aferni. Intech **225** (2022).
38. J.C. Nolasco, J.T. García, A. Castro-Chacón, A. Castro-Carranza, J. Gutowski, AIP Adv. **12**, 025213 (2022)
39. C. E. Chandra, (2022).
40. Pal, J. Mech. Contin. Math. Sci. **16**, (2021)
41. G. Cacciapaglia, C. Cot, F. Sannino, Sci. Rep. **11**, 1 (2021)
42. J. Xue, T. Yabe, K. Tsubouchi, J. Ma, and S. Ukkusuri, Proc. ACM SIGKDD Int. Conf. Knowl. Discov. Data Min. 4279 (2022)
43. B. Shayak, M.M. Sharma, M. Gaur, A.K. Mishra, Int. J. Infect. Dis. **104**, 649 (2021)
44. K. Ghosh, A.K. Ghosh, Nonlinear Dyn. **109**, 47 (2022)
45. G. Perakis, D. Singhvi, O. Skali Lami, L. Thayaparan, Prod. Oper. Manag. (2022).
46. T. Hao, MedRxiv **2019**, 2020.02.26.20028571 (2020).
47. P. Grinchuk, S. Fisenko, Quant. Biol. **10**, 150 (2022)
48. J. Peyrelasse, M. Moha-Ouchane, C. Boned, Phys. Rev. A **38**, 4155 (1988)
49. S.K. Mehta, S. Sharma, J. Colloid Interface Sci. **296**, 690 (2006)
50. E. Procedure, **38**, (1988).
51. M.P. da SiIva, S.N. Cavalcanti, A.M. Alves, D.M.G. Freitas, P. Agrawal, E.O. Vilar, T.J.A. de Mélo, Polym. Eng. Sci. **61**, 2105 (2021)
52. A.L. Navarro-Verdugo, F.M. Goycoolea, G. Romero-Meléndez, I. Higuera-Ciapara, W. Argüelles-Monal, Soft Matter **7**, 5847 (2011)
53. I. Erukhimovich and M. O. de la Cruz, 2319 (2004).
54. J. Trögl, K. Benediktová, Int. J. Environ. Res. **5**, 989 (2011)

55. L. Haanstra, P. Doelman, J.H.O. Voshaar, Plant Soil **84**, 293 (1985)
56. S. Goutelle, M. Maurin, F. Rougier, X. Barbaut, L. Bourguignon, M. Ducher, P. Maire, Fundam. Clin. Pharmacol. **22**, 633 (2008)
57. C.Y. Scovil, J.L. Ronsky, J. Biomech. **39**, 2055 (2006)
58. J. Berkson, J. Am. Stat. Assoc. **39**, 357 (1944)
59. D.M. Ober, N.C. Maynard, W.J. Burke, J. Geophys. Res. Sp. Phys. **108**, 1 (2003)
60. X. Yao, S.J. Titus, S.E. MacDonald, Can. J. For. Res. **31**, 283 (2001)
61. M.K. McAllister, G.P. Kirkwood, ICES J. Mar. Sci. **55**, 1031 (1998)
62. https://coronavirus.jhu.edu/map.html
63. K. Juni, Farumashia **31**, 913 (1995)
64. L. Danon, L. Lacasa, E. Brooks-Pollock, Philos. Trans. R. Soc. B Biol. Sci. **376**, 20200284 (2021)